Physica B 657 (2023) 414757

Contents lists available at ScienceDirect

Physica B: Condensed Matter

journal homepage: www.elsevier.com/locate/physb

Hyperfine properties at Zr sites of Zr-based compounds. A DFT FP-LAPW and GIPAW study

ARTICLE INFO

Keywords
Density functional theory
Electric field gradient
Nuclear quadrupole moment
FP-LAPW
GIPAW
Electronic structure

ABSTRACT

We report Density Functional Theory calculations for the atomic positions and the electric-field gradients (EFG) at Zr sites in a series of Zr compounds, with the FP-LAPW and the GIPAW methods. These data are used to obtain a value for the nuclear quadrupole moments of ^{90}Zr and ^{91}Zr, of which the precision and reliability with respect to tabulated values is discussed. An error bar on our suggested values is provided. Good agreement is obtained between the (faster) GIPAW method and (slower yet established) FP-LAPW method, especially when identical atomic positions are imposed. This increases the confidence in GIPAW calculations for electric-field gradient and nuclear quadrupole moment determination.

1. Introduction

One way to investigate structural, electronic, and magnetic properties at the atomic scale is by using hyperfine techniques [1], such as Nuclear Magnetic Resonance (NMR [2]), Mössbauer spectroscopy [3,4], Time Dependent Perturbed Angular Correlations or Time Dependent Perturbed Angular Distributions (TDPAC and TDPAD [1]), among others. In these techniques, a suitable probe-nucleus of an indigenous atom or an impurity adequately introduced in the system under study senses its electronic and magnetic environment, at the subnanoscopic scale, enabling the characterization of atomic sites in a molecule or a solid system, even when the concentration of those atoms is very low (see, for example, Refs. [5] and [6] and References therein). The information provided in these experiments is given as a product of a property related to the nucleus and another associated with the electronic cloud [1–4]. In the case of pure electric quadrupole interactions, the nuclear property is the nuclear quadrupole moment Q, characteristic of the considered nuclear state with spin I, which interacts with the electric field gradient (EFG) generated by the electron cloud at the nuclear site. Mathematically, the EFG is a traceless symmetric tensor whose components V_{ij} are defined as the second partial-derivatives of the Coulomb potential $V(\boldsymbol{r})$ with respect to the spatial coordinates, evaluated at the nuclear site. In its principal axis system (PAS), the three diagonal components of the EFG follows the convention $|V_{XX}|<|V_{YY}|<|V_{ZZ}|$. Given that $V_{XX}+V_{YY}+V_{ZZ}=0$, the EFG is completely defined by five parameters: the largest component V_{ZZ}, the asymmetry parameter defined as $\eta = (V_{XX} - V_{YY})/V_{ZZ}$ and the Euler angles that define the orientation of the PAS with respect to the lab frame. For $I = 5/2$ and polycrystalline samples, the experimentally measurable quantities are η and the quadrupole coupling constant C_Q defined as

$$C_Q = \frac{eQ}{h} V_{ZZ} \tag{1}$$

where e is the electron charge, h is Planck's constant and Q the nuclear quadrupole moment of the relevant nuclear level. Although C_Q and η contain all the information related to the electronic environment of the probe atom, the interpretation of C_Q and η is not always straightforward and a comparison with independent *ab initio* calculations is essential to improve, reinforce or refute the conclusions obtained from the experiments. Nowadays, these calculations can be efficiently performed in framework of Density Functional Theory (DFT).

It is clear from eq. (1) that for a correct comparison between computation (V_{XX}, V_{YY}, V_{ZZ}) and experiment (C_Q, η), the knowledge of accurate and precise nuclear-quadrupole moments is indispensable. However, for many important probe nuclei, the Q values are not known or are known with limited accuracy and/or precision and their determination is still an active research field [7–11] that gives rise to ~~a~~ new applications of hyperfine techniques and DFT-calculations: the determination of nuclear quadrupole moments from experimentally determined C_Q values at a given probe-site of a molecule or crystal and the computation of the EFG at the same site. This approach provides independent and useful information to nuclear physicists to check nuclear models, joining solid state physics, hyperfine techniques, DFT-based calculations, and nuclear physics [12]. In the last two decades, the increase of computational power, the development of new electronic structure codes for the calculation of the EFG through *ab-initio* or quantum chemistry methods [13] and improvements in the experimental techniques allows the determination of nuclear quadrupole moments of fundamental or excited nuclear states accurately and with very low uncertainness [6,12,13]. The uncertainty of the obtained quadrupole moments when this procedure is used was extensively discussed for the ^{111}Cd probe [6,12,13].

Among the hyperfine spectroscopies, solid-state NMR [2,14] is a versatile method for the hyperfine characterization of molecules and solids [14,15]. One of the five naturally occurring isotopes of Zr, ^{91}Zr, is known as a possible NMR probe. ^{91}Zr is often considered a "challenging nucleus" for NMR experiments due to its low natural abundance, small gyromagnetic ratio, and (particularly) the relatively small nuclear quadrupole moment of the sensitive state (the $5/2^+$ ground state). For these reasons, in the past, the ^{91}Zr-NMR studies were limited to highly symmetric systems, such as metals and Laves-phase materials. In the last three decades, progress in the experimental setup and in the theoretical

https://doi.org/10.1016/j.physb.2023.414757
Received 12 September 2022; Received in revised form 17 February 2023; Accepted 18 February 2023
Available online 2 March 2023

methods for the analysis of the experimental spectra extended the applications of ^{91}Zr-NMR.

The improvement of ^{91}Zr-NMR spectroscopy allows to extend the field of studies to include Zirconium and Zr-based materials with several desirable properties for a large variety of applications. Just to mention a few examples, one of the most important applications of zirconium is in the nuclear industry [16–18]. Also, ZrO_2 (zirconia) is an excellent refractory material and has found many applications in high-temperature environments and as a solid-state electrolyte in solid oxide fuel cells [19]. The hardness and chemical stability of zirconia made this material well suited for ceramic biomaterials [20]. Besides, Zr-ceramics with the perovskite-like crystal structure (perovskite zirconates) exhibit great thermal properties at high temperatures, being therefore promising candidates for high-temperature applications (gas turbine engines at elevated working temperatures [21], aerospace industry [22]). Perovskite zirconates can be also used as solid-state proton conductors [23], ceramic capacitors [24], refractory material [25], and luminescence materials [26,27]. Finally, Na_2ZrO_3 is a material that could be used for CO_2 high-temperature capture technology [28–30].

Another Zr-isotope, ^{90}Zr, can be used as a probe nucleus in Time-Dependent Perturbed Angular Distribution (TDPAD) spectroscopy [31]. The use of ^{90}Zr is less common and very few experiments have been performed. To the best of our knowledge, reported experiments were done only in metals and generally at high temperature (300 K).

Considering the variety of properties and applications of Zr-based materials, and the relevance that the combination of theory and experiment has in the design and understanding of new materials, it is important to validate the precision and accuracy of the theoretical methods and approximations used for the description of the different properties of these compounds. In the present work, we combined theoretical results obtained using two different DFT methods and different approximations for the exchange-correlation functional with experimental results obtained in metallic Zr as well as in Zr-compounds to study the hyperfine properties at the Zr sites. First, we determine the EFG tensor at the Zr sites of α-Zr using the well-established full-potential linearized augmented plane-waves (FP-LAPW) method [32,33]. These predictions are compared with experimental results obtained at low temperature at ^{90}Zr and ^{91}Zr nuclei in metallic Zr to "calibrate" our calculations and to obtain the nuclear quadrupole moments of the $5/2^+$ ground state of the ^{91}Zr NMR level and of the 3589 keV 8^+ excited state of ^{90}Zr (for TDPAD). Thereafter we looked more closely at the EFG at Zr sites in Zr-oxides and -compounds. For these calculations we considered different approximations for the XC functional, and we will discuss to what extent each XC-approximation agrees on the EFG's at the Zr sites. Also, we performed calculations using the Gauge-Including Projected Augmented Waves (GIPAW) method [34,35] implemented in the Quantum Espresso code [36]. One of the goals of this work is to analyze the performance of the GIPAW method for the computation of the EFG at the site of a heavy nucleus (Zr). Since two isotopes are used as probes in NMR and TDPAD experiments, the availability of experimental EFG determinations makes Zr-systems very suitable to assess the accuracy of the GIPAW method for EFG's.

2. Theoretical approach

To obtain the EFG tensor at the Zr sites of α-Zr, scalar relativistic full potential linearized augmented plane-wave (FP-LAPW) calculations were performed using the WIEN2k code [37]. The basis set was composed by more than 330 plane waves plus 25 local orbitals (R_{MT}. $K_{\max} = 10$, with R_{MT} the smallest muffin-tin radius and $K_{\max}$ being related to the plane-wave cutoff). The reciprocal space was described using a dense mesh-grid of 100,000 k-points (4640 k-points in the irreducible first Brillouin zone) and the muffin-tin radius for Zr was set to 1.3 Å. The XC functional considered were the local density approximation (LDA, Ref. [38]), and two parameterizations of the semi-local general gradient approximations: the Perdew−Burke−Ernzerhof (PBE-GGA [39]) and the Wu-Cohen (WC-GGA [40]). Also "beyond-GGA" models for the XC functional were considered: the Becke Johnson potential (BJ [41]) and three parameterizations of the Tran-Blaha modified Becke-Johnson potential (TB-mBJ): the original TB-mBJ [42], and the parameterizations of TB-mBJ proposed by Koller et al. (TB-mBJ12a and TB-mBJ12b [43]).

For the study of the EFG at Zr sites in semiconducting Zr-compounds, initially we performed FP-LAPW calculations using very well converged basis sets ($R_{MT}K_{max} = 8$). The reciprocal space was described using a dense mesh of 500–1000 k-pointd. The same XC-functionals mentioned hereabove were used. In all cases, lattice parameters were fixed at the experimental ones and internal atomic positions have been optimized.

In addition to the well-established all-electron approaches (as the FP-LAPW method), we performed GIPAW calculations. GIPAW is based on the Projector Augmented Wave (PAW [44]) pseudopotentials methodology. In this framework, the pseudopotential replaces the real potential in the atomic core regions. The pseudization allows DFT calculations that are computationally more efficient than the all-electron ones [45] and therefore computational times are drastically reduced in comparison with all-electron methods. For this reason, GIPAW could be an alternative to all-electron methods for the study of complex systems (for example, systems with hundreds or even thousands of atoms). An important issue of GIPAW is that the all-electron wave-functions are reconstructed from the pseudopotentials [35], enabling the calculation of the EFG and other hyperfine parameters with, in principle, the same accuracy as for the all-electron methods [46–48]. This is, however, no common practice yet for the prediction of EFG's in crystals. So, a second objective of this work is to perform GIPAW calculations of the EFG at Zr sites in Zr-compounds to compare the obtained predictions with those obtained using the FP-LAPW method, and with the experimental ^{91}Zr-NMR results. The GIPAW calculations presented here were performed using the pseudopotential and plane-wave (PP-PW) method as implemented in the open-source Quantum-Espresso (QE) code [36]. We have considered Projector Augmented Wave (PAW) pseudopotentials from the Standard Solid-State Pseudopotential library (SSSP) [48,49], and the PBE-GGA [39] XC-functionals. The kinetic energy cutoff for the wave-function and charge density were set to 90 Ry and 900 Ry, respectively. The reciprocal space was described using the Monkhorst-Pack scheme, with a dense grid of k-points equivalent to the grid used in the FP-LAPW method. With these parameters, the numerical precision is close to those achieved in the FP-LAPW calculations.

For the GIPAW calculations the lattice parameters of the Zr-compounds were taken to be the same for FP-LAPW (the experimental ones) while atom positions were optimized separately for both codes, unless noted otherwise.

3. Results and discussions

3.1. EFG at Zr sites in α-Zr

In this section, we will concentrate on the case of metallic Zr. For a fair theory-experiment comparison we select available experimental information on structural parameters and nuclear quadrupole coupling constants C_Q obtained at the lowest measurement temperatures.

Zirconium crystallizes in two different crystal structures. The high-temperature (β-Zr) phase is a body-centered cubic (BCC) crystal structure while the lower temperature (room temperature and below) phase presents the hexagonal close package (HCP) structure (α-Zr). The space group of α-Zr is $P6_3/mmc$ (number 194) and the unit cell contains two Zr atoms located at Wyckoff positions (1/3, 2/3, 1/4) and (2/3, 1/3, 3/4). DFT can predict ground-state lattice parameters accurately. So, it is possible to determine the ground-state lattice parameters of α-Zr from DFT calculations and then calculate the EFG tensor at the Zr sites using this predicted structure. But, in the present work, we are looking for an EFG value that comes as close as possible to the experimental one. For this reason, we will use the experimental lattice parameters that

correspond to the temperature at which the C_Q was measured (in the range 1–4 K) and compute the EFG for that lattice. Later, we will study the influence on the EFG values of slight c/a variations. Experimental values for the lattice parameters of α-Zr at 4.2 K and 300K, obtained from the literature [50,51], are show in Table 1.

The obtained results for V_{ZZ} considering the lattice parameters corresponding to 4.2 K are in the range 4.26–4.29 $\times$ 10^{21} V/m^2, depending on the choice for the XC. In all cases and according to the site symmetry, $\eta = 0.00$. These results are in good agreement with those reported by Blaha et al. in his pioneering work on DFT calculations of the EFG in HCP metals [52]. Using the lattice parameters corresponding to $T = 300$ K, we obtained $V_{ZZ} = 4.23 \times 10^{21}$ V/m^2 (lattice parameters reported by Goldak et al. [50]) and $V_{ZZ} = 4.24 \times 10^{21}$ V/m^2 (lattice parameters reported by Easton et al. [51]). Both these EFGs are obtained with the WC-GGA XC-functional.

An important point related to the calculation of the EFG is the error bar associated with the predicted V_{ZZ} values. To determine this error bar, we considered different sources that contribute to the error budget.

- Numerical error: based on a detailed convergence study, varying the basis set, the number of k-points considered for the sampling of the Brillouin zone and the muffin tin radius we determine that the numerical error in V_{ZZ} is smaller than 0.02 $\times$ 10^{21} V/m^2 (relative error below 0.5%) for R_{MT}. $K_{max} = 10$ and the mesh-grid of 100,000 k-points.
- Error associated with the XC-functional: by taking the average V_{ZZ} value obtained for the structure determined at 4.2 K, (4.27 $\times$ 10^{21} V/m^2) we established an error bar of $\pm$0.02 $\times$ 10^{21} V/m^2.
- Lattice parameters: One source of uncertainty on the EFG predictions is the choice of the lattice parameters and, particularly for the HCP metals, the value of the c/a ratio. To evaluate the error associated with the lattice parameters we have calculated the EFG for several c/a ratios in an interval of $\pm$0.50% around the experimental c/a ratio measured at 4.2 K keeping the cell volume fixed. These changes in the c/a ratio implies that a and c changes $\pm$0.005 and $\pm$ 0.015 Å, respectively. This interval largely covers the usual error bars in the experimental determination of the lattice parameters. When the c/a ratio is increased/decreased keeping fixed the cell volume, the WC-GGA calculations predict $V_{ZZ} = 4.01 \times 10^{21}$ V/m^2 (when c/a is increased 0.50%) to $V_{ZZ} = 4.54 \times 10^{21}$ V/m^2 (when c/a is decreased 0.50%). A linear dependence of V_{ZZ} with c/a can be seen in Fig. 1. To determine the linear dependence of the EFG with c/a in Fig. 1 we include calculations extending the c/a variation interval up to 1%. On the other hand, when the cell volume is increased/decreased 0.50% with c/a ratio fixed at the experimental value obtained at 4.2. K the WC-GGA calculations predicts $V_{ZZ} = 4.24 \times 10^{21}$ and 4.30 $\times$ 10^{21} V/m^2, showing that the c/a ratio play the fundamental role on for the EFG dependence on a and c.

Finally, we also performed a calculation including spin−orbit coupling. As in the case of other host lattices with heavy elements (HCP–Cd and HCP-Hg) [6], we found a negligible effect on V_{ZZ} for the case of Zr. Therefore, no error bar contribution due to spin−orbit coupling was considered.

Based on this discussion a conservative error bar of $\pm$0.30 $\times$ 10^{21} V/m^2 can be established for the EFG at the Zr sites of α-Zr, and we conclude that the DFT-predicted EFG at 4.2 K is 4.27 (30)x10^{21} V/m^2, $\eta = 0.00$.

Now we can compare our results for the EFG at Zr sites of α-Zr with

Table 1
Experimental lattice parameters of α-Zr at 4.2 and 300 K.

Temperature (K)	a (Å)	c (Å)	c/a	Reference
4.2	3.2294	5.1414	1.5921	[50]
300	3.2331	5.1491	1.5926	[50]
300	3.2327	5.1471	1.5922	[51]

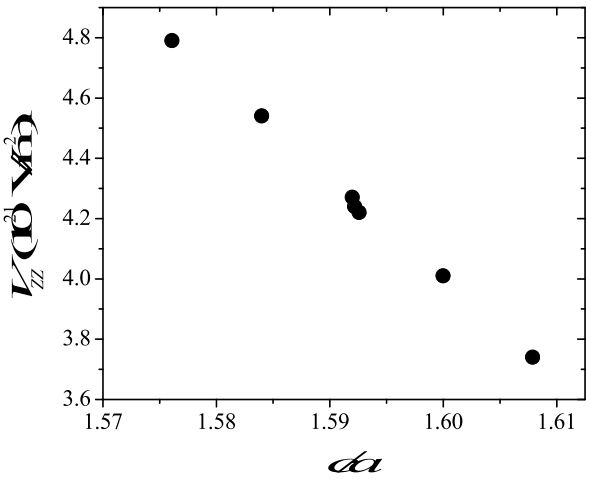

Fig. 1. Main component of the EFG tensor, V_{ZZ}, as a function of the c/a ratio (cell volume fixed).

the experimental ones. The experimentally determined magnitude is the quadrupole coupling constant C_Q, related to V_{ZZ} according to eq. (1). Since our calculations correspond to 0K we will use low-temperature experiments. We can use the C_Q values obtained in two experiments reported in the literature. In the first one, NMR for ^{91}Zr (5/2$^+$ ground state) in α-Zr has been performed in the temperature range 1.4–4.2 K and in the frequency range of 15–30 MHz by the pulsed nuclear resonance technique. The resonance spectra obtained are well-resolved spectra and correspond to a pure nuclear electric quadrupole interaction. The quadrupole coupling constant was determined to be $C_Q(^{91}\text{Zr})$ = 18.7 (3) MHz [53]. In the second experiment, C_Q at ^{90}Zr sites of α-Zr was determined by TDPAD (3589 keV 8$^+$ excited state, $t_{1/2} = 135$ ns). The reported result is $C_Q(^{90}\text{Zr}) = 45.5$ (4) MHz [54]. This result was obtained by extrapolation to 0K using the $T^{3/2}$ dependence of the EFG observed in metals [55].

To compare these experimental results with the theoretical ones we have to "translate" the $C_Q(^{90}\text{Zr})$ and C_Q (^{91}Zr) values to $V_{ZZ}(^{90}\text{Zr})$ and $V_{ZZ}(^{91}\text{Zr})$. To obtain these "experimental EFGs", it is mandatory to have precise knowledge of the nuclear quadrupole moment Q of the sensitive states involved in the experimental determinations. This point is usually the bottleneck: The nuclear quadrupole moments are known with limited accuracy or different values are reported in the literature. In the case of the Q value of the 5/2$^+$ ground state of ^{91}Zr NMR-probe, up to the year 2000, different works reported Q values in the range −0.206 to −0.257 b. In 1982, Büttgenbach et al. [56] used experimental data for several states of atomic Zr having $4d^{N-2}5s^2$ and $4d^{N-1}5s$ configurations. The electric field gradient was obtained via a parameter fit from the $<r^{-3}>$ of the magnetic dipole hyperfine interaction. The reported result was Q (^{91}Zr) = -0.206 (10) [56]. After that, in 1993, Young et al. [57] reported an experimental and theoretical study of the hyperfine structure of various metastable levels of 91Zr. The hyperfine structures arising from the 4d3 and 4d25s configurations were measured using the laser-rf double-resonance method in a collinear laser–ion-beam geometry and combined with a relativistic configuration-interaction (RCI) approach and independent-particle Dirac-Fock (DF) calculations. The result for Q (^{91}Zr) was −0.257 (13) b. Five years after this determination, Bouazza et al. [58] used parameter fits for the Zr atom in the $(4d+5s)^4$ model space and obtained Q (^{91}Zr) = -0.230 (20) b. None of these determinations is very accurate, especially when handling dynamic correlation and core polarization (Sternheimer) effects.

The most reliable and precise value for Q (^{91}Zr) was obtained by V. Kellö et al. [59]. In this case, the Q value was derived from high-resolution microwave spectra of diatomic ZrO and ZrS molecules. The obtained C_Q value was combined with quasi-relativistic Douglas–Kroll calculations at levels up to Coupled Cluster Single-Double and

Perturbative Triple method, CCSD-T, yielding Q (^{91}Zr) = −0.176 (3) b. This value (that is not based on other Q values and is much smaller than the available "atomic" ones previously presented) is supported by fully relativistic CCSD-TT calculations using a slightly smaller basis.

In the case of ^{90}Zr, there are two works that report the nuclear quadrupole moment Q of its 3589 keV 8^+ excited state, Raghavan et al. [60]. and Bendahan et al. [61]. In the first case, static quadrupole moments of ^{90}Zr (and other 8^+ and $21/2^+$ isomers) were measured using TDPAD technique. The isomers were excited by pulsed heavy-ion beams and recoil implanted into single crystals of Zr in which their quadrupole precession was determined. The reported result is Q (^{90}Zr) = +0.51 (3) b. In the second work, the sign of the nuclear quadrupole moments of ^{88}Zr and ^{90}Zr were measured by tilted multifoil technique. This is a more complicated experiment with much less statistics, that prevented the authors to really fit the quadrupole coupling constant value and their goal was to determine the sign of the nuclear quadrupole moments. In fact, they took the C_Q value from Raghavan's paper [54], fixed it for their fit, and checked afterwards that when they let it free again, it did not change considerably. From the experimental results Bendahan et al. showed that the signs of the nuclear quadrupole moments of ^{88}Zr and ^{90}Zr are opposite. To determine the absolute sign of each nuclear quadrupole moment the authors assumed a positive sign for the EFG at the Zr sites of HCP-Zr. This assumption was based on a non-conclusive reasoning but was later confirmed by the DFT calculations by Blaha et al. [52]. Shell model calculations reported in Ref. [61] yield Q(^{90}Zr) = -0.504 b, which in value and in sign agree with the quadrupole moment reported in Refs. [60,61].

In Fig. 2 we present the experimental V_{ZZ} values at ^{91}Zr sites in α-Zr obtained using the different Q values reported in the literature previously discussed. As can be seen, our *ab-initio* results are in good agreement with the experimental result if the most reliable Q value, Q (^{91}Zr) = −0.176 (3) [59], is used to obtain the experimental V_{ZZ} value. In an alternative way, we can use our results for V_{ZZ} in combination with the experimentally reported C_Q value to determine Q (^{91}Zr), obtaining Q (^{91}Zr, FP-LAPW) = −0.181 (9) b, irrespective of the XC-functional employed. The error bar in Q (^{91}Zr) is originated by both the error associated to V_{ZZ} (see previous section) and the error bar associated to the experimental determination of C_Q. Our result is very similar to the most reliable, precise, and recommended value, Q (^{91}Zr) = -0.176 (3) b reported by Kellö et al. [59]. Nevertheless, there is useful information emerging from a comparison between our Q (^{91}Zr) = −0.181 (9) b and the value by Kellö et al. The reason why the value obtained by Kellö et al. is more precise and more reliable is that it is determined by comparing quadrupole coupling constants obtained by high-resolution microwave spectroscopy on diatomic molecules, and high-level quantum-chemistry calculations of the EFG for these same molecules. Unlike DFT, the post-Hartree-Fock calculations used in quantum chemistry are not limited by the uncontrolled uncertainty that is introduced by the choice of an XC-functional. Even when several XC-functionals are used to assess their possible spread, as was done in the present work, and when they are found to be in good agreement with each other, there is no guarantee that the obtained predictions for the EFG come anyhow close to the true value. By comparing the experimental quadrupole coupling constant for ^{91}Zr in hcp-Zr (18.7 (3) MHz, Ref. 53) with the quantum chemistry Q (^{91}Zr) = -0.176 (3) b, V_{ZZ} in hcp-Zr can be determined to be 4.39 (7) x10^{21} V/m^2. This value must be compared to our direct and entirely independent DFT value of 4.27 (30)x10^{21} V/m^2: the DFT value for the EFG is 3% smaller than the value determined via quantum chemistry. A similar conclusion was obtained for the EFG at the Cd site in hcp-Cd [6, 62]. Also, in Ref. [6] a few other cases were indicated that point to the same trend: DFT calculated EFGs are a few percent smaller than EFGs determined via quantum chemistry. We recommend further investigations to find out whether this is a general rule or rather a coincidence due to a small number of examples.

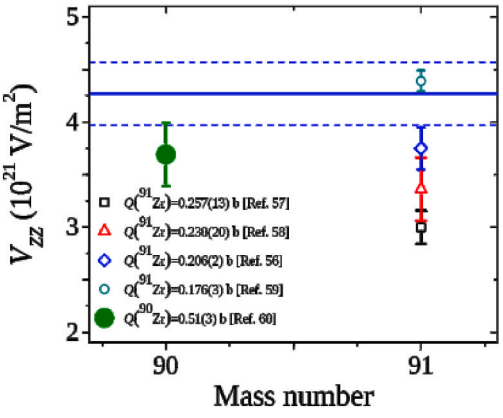

Fig. 2. Experimental V_{ZZ} determined from ^{90}Zr (solid green circle) and ^{91}Zr C_Q data (open forms) using eq. (1) and considering the different reported Q (^{91}Zr) values. The blue solid line represents the DFT prediction (4.27 × 10^{21} V/m^2) obtained in the present work. Dashed blue line indicates the error bar associated to the calculated V_{ZZ} values (0.3 × 10^{21} V/m^2).

As can be seen in Fig. 2, the agreement between the experimental V_{ZZ} value obtained using the reported value for Q (^{90}Zr), 3.69 × 10^{21} V/m^2, and the DFT prediction is poor. We must notice here that the experimental V_{ZZ} value must be independent of the mass number of the probe-isotope. Using eq. (1) and the fact that V_{ZZ}(^{90}Zr) = V_{ZZ}(^{91}Zr) in the same host we obtain:

$$Q\left(^{90}Zr\right) = Q\left(^{91}Zr\right)\frac{C_Q\left(^{90}Zr\right)}{C_Q\left(^{91}Zr\right)} \quad (2)$$

Using the experimental result C_Q(^{90}Zr) = 45.5 (4) MHz [54] and C_Q(^{91}Zr) = 18.7 (3) MHz [53] we obtain Q (^{90}Zr) = 0.44 (3) b (using our Q (^{91}Zr) value) or Q (^{90}Zr) = 0.43 (1) b, considering the Q (^{91}Zr) reported by Këllo et al. [59], evidencing a discrepancy with the Q (^{90}Zr) reported by Raghavan et al., Q (^{90}Zr) = 0.51 (3) b [60]. Up to 2017, this value was the tabulated one (see Refs. 8 and 9), and therefore the recommended value. In the 2021 version of the table [10], the recommended value became Q (^{90}Zr) = -0.44 (3) b, but still referencing the works of Ravhagan et al. [60] and Bendahan et al. [61], references in which this value did not explicitly appear. The explanation for this change in the tabulated value is that Eq. (2) hereabove has been applied, with the new value Q(^{91}Zr) = -0.176 (3) b for the reference isotope ^{91}Zr.

3.2. FP-LAPW predictions for the EFG at Zr sites of Zr-compounds

After the study of metallic Zr we pay attention to the EFG at Zr sites in semiconducting Zr-compounds. To this aim, we selected ten Zr-systems with semiconducting character (Zr-oxides in four different phases: zircon; $AZrO_3$-systems with perovskite structure, A: Ba; Ca; Sr, Na_2ZrO_3 and Na_2ZrSiO_5). For all these systems accurate structural data (see Table 2) and ^{91}Zr-NMR measurements are reported in the literature. Also, these set of systems enable us to cover EFG values that range from 0 to 30 × 10^{21} V/m^2.

Before presenting our results and comparing them with the experimental ones, there are some points that must be considered for a realistic comparison theory/experiment. Firstly, our calculations correspond to 0K. But, the experimental results for the Zr-compounds that will be discussed here were obtained at 300 K. Consequently, thermal effects not included in the DFT calculations could produce a deviation of our predictions from the experimental results. Additionally, in some cases, there are experimental issues that must be considered. For example, the ^{91}Zr NMR spectra of Na_2ZrSiO_5 are indicative of one crystallographic Zr site [15], while XRD experiments suggest the presence of two similar Zr sites that must exhibit similar C_Q and η parameters. In the case of Na_2ZrO_3, its crystal structure is characterized by two sites for the Zr atoms (site 1 and site 2). The measured ^{91}Zr spectrum revealed a high

Table 2
Experimental structural data reported in the literature for the Zr-based compound considered in this study.

Compound	Space group	Structural parameters	Reference
c-ZrO_2	$Fm3m$	$a = 5.1429$ Å	[63]
t-ZrO_2	$P4_2/nmc$	$a = 3.6084$ Å, $c = 5.1771$ Å	[64]
o-ZrO_2	$Pbc2_1$	$a = 5.0680$ Å, $b = 5.2600$ Å, $c = 5.0770$ Å	[19]
m-ZrO_2	$P2_1/c$	$a = 5.1429$ Å, $b = 5.2077$ Å, $c = 5.3195$ Å, $\beta = 99.2°$	[64]
$ZrSiO_4$	$I4_1/amd$	$a = 6.6039$ Å, $c = 5.9783$ Å	[65]
$CaZrO_3$	$Pcmn$	$a = 5.5974$ Å, $b = 8.0271$ Å, $c = 5.7691$ Å	[25]
$BaZrO_3$	$I4/mcm$	$a = 5.8722$ Å, $b = 8.3577$ Å	[66]
$SrZrO_3$	$Pbnm$	$a = 5.7920$ Å, $b = 5.8130$ Å, $c = 8.1960$ Å	[67]
Na_2ZrO_3	$C12/c1$	$a = 5.5230$ Å, $b = 9.7490$ Å, $c = 11.1270$ Å, $\beta = 99.98°$	[68]
Na_2ZrSiO_5	$P2_1/c$	$a = 13.8840$ Å, $b = 5.4750$ Å, $c = 13.6980$ Å, $\beta = 119.83°$	[69]

degree of crystallinity and was fitted with one hyperfine interaction, suggesting a similar environment for the Zr ions in both structural sites [15]. In the case of orthorhombic ZrO_2 (o-ZrO_2), the ^{91}Zr NMR experiment revealed the presence of disorder, even though the sample is crystalline. This disorder is attributed to the presence of Y_2O_3 added to stabilize this phase at low temperature [15]. Similarly, the tetragonal phase of ZrO_2 (t-ZrO_2) contains significant amounts of the orthorhombic phase, leading to some degree of disorder in the Zr neighborhood [15].

In Table 3 we present our FP-LAPW results for V_{ZZ} and η for the selected Zr-systems and for the different XC approximations employed. From this table some general conclusions can be obtained. As it can be seen, the three parameterizations of the TB-mBJ functional yield very similar results for V_{ZZ} and η. Similarly, the GGA approximation predicts V_{ZZ}'s and η's that are very similar to those obtained in the framework of the BJ calculations. Also, the GGA and BJ V_{ZZ} values are generally slightly larger than the TB-mBJ ones. Another result is related to the two structural sites for the Zr ions of Na_2ZrO_3 and Na_2ZrSiO_5. As it can be seen in Table 3, irrespective of the XC approximation employed, the V_{ZZ} and η values at both inequivalent Zr sites of Na_2ZrO_3 are very similar. This theoretical result for V_{ZZ} is in excellent agreement with the experimental one that reveals a unique hyperfine interaction in the ^{91}Zr spectra of Na_2ZrO_3. In the case of Na_2ZrSiO_5, the hyperfine interactions at both Zr sites are characterized by calculated V_{ZZ} values that differ less than 7% and, also a difference in the η value for sites 1 and 2 is predicted (see Table 3). These differences imply that the two hyperfine interactions must be distinguishable in the ^{91}Zr-NMR experiment. However, depending on the quality of the sample and the resolution of the spectrometer these interactions might not be resolved.

Now we can compare our theoretical results with the experimental ones [14,15]. To this purpose we obtained the experimental V_{ZZ} values using $V_{ZZ}^{exp} = (h/Qe)C_Q$ with $Q = 0.181$ (9) b. As can be seen in Table 3, a good agreement between FP-LAPW predictions and experiments is observed, with exception of t-ZrO_2 and Na_2ZrSiO_5. As a general trend, the TB-mBJ results for V_{ZZ} and η are in better agreement with the experimental results than those obtained with the GGA and BJ approximations, but even these results are in good agreement with the experimental ones. The disagreement between theory and experiment in the case of t-ZrO_2 can be associated to the disorder and the presence of spurious phases introduced by the doping process of the host sample to stabilize the tetragonal phase at room temperature. In the case of Na_2ZrSiO_5, this compound presents a complex structure, so a refinement of the structural data could be necessary for a better prediction. Also, new experiments would be of interest to better understand the origin of the discrepancy theory-experiment.

For a deeper comparison between theory and experiment, we plot in Fig. 3 the EFG values obtained by our FP-LAPW calculations as a function of the experimental C_Q values. In this figure, the red lines correspond to a linear fit to the data set considering all the systems studied here. The blue lines correspond to linear fits excluding the suspicious t-ZrO_2 and Na_2ZrSiO_5 points. As can be seen, a linear correlation is observed in all cases. The best linear correlation is obtained for TB-mBJ calculations, irrespective of the parameterization considered. The results of the fitting procedure are reported in Table 4.

As it has been emphasized by Thierfelder et al. [70], additionally to

Table 3
Quadrupole coupling constant C_Q obtained in ^{91}Zr-NMR experiments performed at 300 K (room temperature), experimental V_{ZZ} values (obtained from C_Q using eq. 1 and $Q(^{91}Zr) = -0.181$ (9) b) and FP-LAPW predictions for V_{ZZ} obtained using the different approximations for the XC potential. The experimental C_Q values can be found in Refs. [14,15]. Lattice parameters were fixed at the experimental ones and internal positions were optimized.

Experimental			$V_{ZZ}^{FP\text{-}LAPW}$				
(10^{21} V/m^2)	C_Q (MHz)	V_{ZZ}^{exp} (10^{21} V/m^2)	WC-GGA	BJ	TB-mBJ09	TB-mBJ012a	TB-mBJ02b
HCP-Zr (α-Zr)	18.7 (3)	4.27 (9)	4.24	4.29	4.28	4.27	4.27
	$\eta = 0.00$	$\eta = 0.00$	$\eta = 0.00$	$\eta = 0.00$	$\eta = 0.00$	$\eta = 0.00$	$\eta = 0.00$
c-ZrO_2	0	0	0	0	0	0	0
	$\eta = -$	$\eta = -$	$\eta = -$	$\eta = -$	$\eta = -$	$\eta = -$	$\eta = -$
m-ZrO_2	23.2 (2)	5.30 (7)	5.6	5.7	5.1	5.2	5.1
	$\eta = 0.10$	$\eta = 0.10$	$\eta = 0.06$	$\eta = 0.04$	$\eta = 0.06$	$\eta = 0.06$	$\eta = 0.11$
t-ZrO_2	19.3 (3)	4.40 (9)	7.0	7.1	5.9	5.7	5.5
	$\eta = 0.00$	$\eta = 0.00$	0.00	0.00	0.00	0.00	0.00
o-ZrO_2	17.9 (9)	4.1 (2)	4.0	4.1	3.8	3.9	3.9
	$\eta = 0.9$ (1)	$\eta = 0.9$ (1)	$\eta = 0.82$	$\eta = 0.68$	$\eta = 0.95$	$\eta = 0.78$	$\eta = 0.84$
$ZrSiO_4$	20.5 (2)	4.68 (7)	5.4	5.3	4.7	4.6	4.5
	$\eta = 0.00$	$\eta = 0.00$	$\eta = 0.00$	$\eta = 0.00$	$\eta = 0.00$	$\eta = 0.00$	$\eta = 0.00$
$CaZrO_3$	8.3 (9)	1.9 (2)	2.6	2.6	1.8	1.7	1.7
	$\eta = 0.5$ (3)	$\eta = 0.5$ (3)	$\eta = 0.49$	$\eta = 0.48$	$\eta = 0.52$	$\eta = 0.51$	$\eta = 0.53$
$BaZrO_3$	0.32 (10)	0.07 (2)	0.8	0.7	0.5	0.7	0.5
	$\eta = 1.0$ (30)	$\eta = 1.0$ (30)	$\eta = 0.00$	$\eta = 0.0$	$\eta = 0.00$	$\eta = 0.00$	$\eta = 0.0$
$SrZrO_3$	4.3 (3)	1.0 (7)	1.3	1.3	1.1	1.0	1.0
	$\eta = 0.6$ (1)	$\eta = 0.6$ (1)	$\eta = 0.08$	$\eta = 0.08$	$\eta = 0.08$	$\eta = 0.10$	$\eta = 0.15$
Na_2ZrO_3	14.5 (5)	3.3 (1)	Site 1: 2.9	Site 1: 3.2	Site 1: 3.0	Site 1: 3.1	Site 1: 3.1
	$\eta = 0.24$ (6)	$\eta = 0.24$ (6)	$\eta = 0.30$	$\eta = 0.29$	$\eta = 0.27$	$\eta = 0.27$	$\eta = 0.27$
			Site 2: 2.9	Site 2: 3.2	Site 2: 3.0	Site 2: 3.1	Site 2: 3.1
			$\eta = 0.29$	$\eta = 0.28$	$\eta = 0.23$	$\eta = 0.23$	$\eta = 0.23$
Na_2ZrSiO_5	29.4	6.72	Site 1: 5.1	Site 1: 5.2	Site 1: 4.1	Site 1: 3.9	Site 1: 3.9
	$\eta = 0.70$	$\eta = 0.70$	$\eta = 098$	$\eta = 0.97$	$\eta = 0.94$	$\eta = 0.90$	$\eta = 0.93$
			Site 2: 4.7	Site 2: 4.8	Site 2: 4.0	Site 2: 3.5	Site 2: 3.8
			$\eta = 0.09$	$\eta = 0.11$	$\eta = 0.08$	$\eta = 0.06$	$\eta = 0.07$

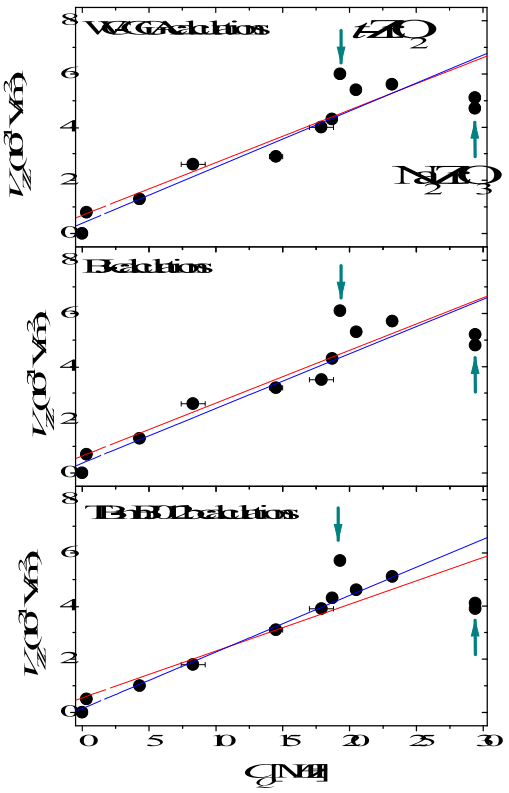

Fig. 3. Theoretically obtained main component of the EFG tensor, V_{ZZ}, as a function of the quadrupole coupling constant C_Q determined by ^{91}Zr-NMR experiments for all the FP-LAPW calculations performed. Red line is the linear fit to all the data set. Blue line is the linear fit excluding t-ZrO_2 and Na_2ZrSiO_5 (indicated by dark cyan arrows).

the slope and the correlation coefficient of the linear fit, also the intercept is a strong quality indicator: if it is not close to zero this indicates a systematic error in the first-principles calculations. In our study, the intercept b with its error bar covers the zero value or is close to it, corroborating the conclusion that there are no systematic additive terms present. A deeper analysis of the fit shows that, when the conflictive systems (t-ZrO_2 and Na_2ZrSiO_5) are excluded, the slope M is not affected (changes in M are smaller than the error bars) but b goes to zero, reinforcing the idea that these experimental determinations present some problem.

Table 4
Results of the linear fits (slope M and intercept b) to the experimental nuclear quadrupole frequency C_Q and computed V_{ZZ} values plotted in Fig. 3. From M, the Q value was derived according to $Q = (e/h).M$ (see eqs. (1) and (3)).

Calculation	Slope M (x10^{13} V/MHz.m^2)	Intercept b (x10^{21} V/m^2)	Q (b)
WC-GGA, considering all Zr-compound	0.20 (4)	0.7 (6)	0.21 (5)
WC-GGA, excluding t-ZrO_2 and Na_2ZrSiO_5	0.21 (2)	0.4 (5)	0.20 (2)
BJ, considering all Zr-compound	0.20 (4)	0.6 (5)	0.21 (5)
BJ, excluding t-ZrO_2 and Na_2ZrSiO_5	0.21 (2)	0.4 (4)	0.20 (2)
TB-mBJ012b, considering all Zr-compound	0.19 (3)	0.5 (6)	0.23 (3)
TB-mBJ012b, excluding t-ZrO_2 and Na_2ZrSiO_5	0.212 (7)	0.1 (2)	0.195 (9)

From the slope M of each linear fit, we can obtain Q but now considering oxides and experiments performed at 300 K. As can be seen in Table 4, the Q values obtained using these experimental data agree with those obtained for the case of α-Zr, the "ideal situation". Leaving aside the physical meaning of the slope of the linear correlation between V_{ZZ} and C_Q, we can consider this slope as calibration factor for ^{91}NMR experiments performed at room-temperature:

$$V_{ZZ} = M.C_Q \tag{3}$$

with $M = 0.21\ (2)\text{x}10^{13}$ V/(MHz.m^2) and C_Q expressed in MHz.

3.3. The EFG at Zr sites of Zr-compounds. GIPAW results

Now we can proceed to analyze the capability of the GIPAW method for the prediction of the EFG at Zr sites in the studied set of Zr-compounds. For simplicity, we will confront the GIPAW results with the TB-mBJ012b ones. As can be seen in Table 5, GIPAW correctly reproduces the experimental and the FP-LAPW results for V_{ZZ} and η values for most cases. Moreover, the GIPAW prediction for V_{ZZ} at the Zr site of t-ZrO_2 is in better agreement with the experimental result than the FP-LAPW ones. In the case of Na_2ZrSiO_5, the GIPAW predictions for the EFG at both inequivalent Zr-sites are far away from the FP-LAPW results, but now the V_{ZZ} values at each site (7.4×10^{21} V/m^2 for site 1 and 5.9×10^{21} V/m^2 for site 2) differ by approximately 25%. This difference must be observed in a ^{91}Zr-NMR experiment. Since the fractions of sites 1 and 2 in the unit cell of Na_2ZrSiO_5 are equal, both interactions should be present with the same intensity. We can note that the average V_{ZZ} value, (V_{ZZ} (site 1) + V_{ZZ} (site 2))/2 = 6.65×10^{21} V/m^2, it is in very good agreement with the experimental V_{ZZ} value (6.72×10^{21} V/m^2). This result suggests that both interactions are not resolved in the experiment (due to the quality of the sample, the resolution of the NMR spectrometer or another kind of effect) and the experimental result in fact correspond to an average value of the interactions associated to each site. A new accurate experiment would be very useful to make a better comparison between the experimental results and the FP-LAPW and

Table 5
Experimental V_{ZZ} values (obtained from C_Q using eq. 1 and $Q(^{91}\text{Zr}) = -0.181$ (9) b) at ^{91}Zr-NMR sites of the studied compounds and the GIPAW and FP-LAPW prediction for V_{ZZ} and η. Columns four and seven correspond to TB-mBJ012b calculations and are repeated from Table 3 for an easy comparison. Calculations were performed keeping the lattice parameters fixed at the experimental ones (see Table 2) and optimizing the internal positions with each calculation method separately.

	V_{ZZ} (10^{21} V/m^2)			η		
	Exp.	GIPAW	FP-LAPW	Exp.	GIPAW	FP-LAPW
HCP-Zr	4.27 (9)	4.30	4.27	0.00	0.00	0.00
***c*-ZrO_2**	0	0	0	–	–	–
***m*-ZrO_2**	5.30 (7)	5.3	5.1	0.10	0.19	0.11
***t*-ZrO_2**	4.40 (9)	4.9	5.5	0.00	0.00	0.00
***o*-ZrO_2**	4.1 (2)	4.4	3.9	0.9 (1)	0.92	0.84
$ZrSiO_4$	4.68 (7)	5.1	4.5	0.00	0.00	0.00
$CaZrO_3$	1.9 (2)	2.3	1.7	0.5 (3)	0.03	0.53
$BaZrO_3$	0.07 (2)	0.12	0.5	1.0	0.00	0.00
$SrZrO_3$	1.0 (7)	1.4	1.0	0.6 (1)	0.88	0.15
Na_2ZrO_3	3.3 (1)	Site 1: 3.4 Site 2: 3.4	Site 1: 3.1 Site 2: 3.1	0.24 (6)	Site 1: 0.22 Site 2: 0.22	Site 1: 0.27 Site 2: 0.23
Na_2ZrSiO_5	6.72	Site 1: 7.4 Site 2: 5.9	Site 1: 3.9 Site 2: 3.8	0.70	Site 1: 0.60 Site 2: 0.41	Site 1: 0.93 Site 2: 0.07

GIPAW calculations.

An inspection of Table 5 reveals that GIPAW and FP-LAPW predict the same EFG's for HCP-Zr (difference of 0.03 × 10^{21} V/m^2, which is below the convergence error of the calculations). In the case of the other Zr-compounds, differences in the EFG predictions obtained by GIPAW and FP-LAPW calculations are in the order of 0.5 × 10^{21} V/m^2. We should note here that the EFG's at the Zr sites were obtained at the slightly different equilibrium structures. The Zr-first neighbour bond-lengths predicted by GIPAW and FP-LAPW differ (in all cases) by less than 0.02 Å. These are very small differences, but due to the extreme sensitivity of the EFG to small changes in the Zr-first neighbour distances and, particularly, in the asymmetry of the local structure around the site in which the EFG is computed, a question arises here: do the differences in the EFG at the Zr sites predicted by GIPAW and FP-LAPW originated in the different local geometries or in the calculation method? To answer this question, and to separate the structural and methodological effects, we have performed GIPAW and FP-LAPW calculations using the same lattice parameters (as we did before) and the same positions of the atoms in the unit cell (fixed at the experimental values, i.e., not doing a position optimization for either code). For all the systems studied here we found that GIPAW and FP-LAPW predict EFG's that differs in less than 0.2 × 10^{21} V/m^2 when the structures are identical. This difference between both calculation method is smaller than the convergence error of the calculations. Then, the differences observed in Table 5 can be associated to the slightly different zero-force atom positions predicted by each calculation and not to a different description of the electronic structure of the system under study made by GIPAW and FP-LAPW.

To illustrate the extreme sensitivity of the EFG to fine details of the local structure around Zr, we selected two systems, *t*-ZrO_2 and $ZrSiO_4$, and we performed various "computational experiments". *t*-ZrO_2 crystalizes in the $P4_2/nmc$ structure with lattice parameters $a = 3.6084$ Å and $c = 5.1771$ Å [64]. The Zr atoms are located at positions ±(3/4; 1/4; 1/4) a the oxygen atoms at ±(1/4, 1/4, u) and ±(1/4, 1/4, ½+u), with $u = 0.0482$ [64], so the unit cell has one internal degree of freedom. Zr atoms are surrounded by eight oxygen atoms (*ONN*), four located at 2.11 Å from the Zr site (d_1), while the other four are located at 2.41 Å (d_2). An increment of 0.001 in u implies a shortening of 0.005 Å of d_1 and the same enlargement of d_2 and the force on the oxygen neighbours changed by 0.05 eV/Å upon displacing oxygen over the same distance. These changes in the Zr-*ONN* bond-lengths generates an increment of 0.2 × 10^{21} V/m^2 in V_{ZZ}. A reduction in the magnitude of V_{ZZ} of 0.2 × 10^{21} V/m^2 occurs when u is reduced by 0.001. In the case of $ZrSiO_4$, its space group is $I4_1/amd$. The structure is characterized by the lattice parameters $a = 6.6039$ Å and $c = 5.9783$ Å. Two parameters determine the positions of the oxygen atoms, $y = 0.06586$ and $z = 0.19533$ [71] (two internal degrees of freedom). The structure has only one crystallographic Zr site, coordinated to four oxygen atoms located at 2.13 Å from the Zr site and four at 2.27 Å. A change of ±0.001 in y (for a fixed z value) produce changes in the order of 0.7 × 10^{21} V/m^2 in V_{ZZ}. Variations of ±0.001 in z (for a fixed y value) produces changes in the order of 0.15 × 10^{21} V/m^2 in V_{ZZ}. The forces on the oxygen atoms varied by 0.15 eV/Å when making these displacements. We conclude from these studies that identical geometries (same size and shape of the unit cell and same positions of the atoms) will provide nearly identical V_{ZZ} values for both FP-LAPW and GIPAW, but that larger differences may occur in crystals where the forces do not strongly increase with displacement, and where therefore a larger variation in predicted equilibrium positions may occur.

In Fig. 4 we plot the GIPAW results for V_{ZZ} as a function of the experimentally determined C_Q. For a better and more clear comparison, we included the results obtained by the TB-mBJ12b FP-LAPW calculations. A linear correlation, with a slope $M = 0.22$ (1)x10^{13} V/(MHz.m^2) and intercept equal to 0.1 (1)x10^{21} V/m^2 is achieved. This result is in excellent agreement with those obtained in the case of the TB-mBJ012b FP-LAPW calculations. The Q value obtained using GIPAW and the experimental results at 300 K is 0.188 (8) b, again in excellent agreement with the FP-LAPW calculations. As in the case of the FP-LAPW calculations, b is zero considering its error bar.

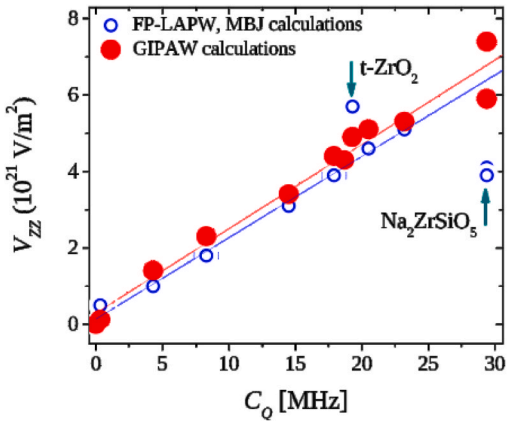

Fig. 4. V_{ZZ} calculated by GIPAW and FP-LAPW (TB-mBJ12b calculations) as a function of the quadrupole coupling constant C_Q obtained in ^{91}Zr-NMR experiments. Red line is the linear fit to all the data set and GIPAW calculations.

4. Conclusions

In this work we have studied, by means of DFT calculations the EFG tensor at the Zr sites of metallic Zr and semiconducting Zr-compounds using different parameterizations for the XC potential: LDA, different parameterizations of GGA and beyond-GGA approximations (BJ, the original TB-mBJ functional proposed in 2009 by Tran and Blaha and the two parameterizations of TB-mBJ proposed by Koller et al., in 2012). Also, the capability of the GIPAW method for the prediction of hyperfine properties, in this case the EFG tensor at the Zr sites, was evaluated.

First, we study the EFG at Zr sites in α-Zr. By combining our results with the experimental C_Q obtained in ^{91}Zr-NMR experiments performed at low temperatures (4.2 K), the nuclear quadrupole moment Q of the 5/2$^+$ ground state of ^{91}Zr was determined to be 0.181 (9) b. By comparing this result with those obtained from quantum chemistry calculations (that are not affected by the systematic error originated by the choice of the XC functional) we conclude that our DFT calculations underestimates the EFG by a few percent (in the order of 3%), and therefore overestimates the quadrupole moment by the same amount. A similar conclusion was obtained in previous works for the case of the EFG at Cd sites in metals and Hg-containing compounds. Based on the result obtained for C_Q in ^{90}Zr-TDPAD experiments the nuclear quadrupole moment of the 3589 keV 8$^+$ excited state of ^{90}Zr was redetermined to be 0.44 (3) b.

Second, we study the EFG in a set of semiconducting Zr-compounds. We found that LDA/GGA and BJ calculations predict similar EFG values. In the case of the different parameterizations of the TB-mBJ approximation for the XC potential, the obtained EFG values are not very sensitive to the parameterization considered. The obtained V_{ZZ} values are smaller than those determined by LDA/GGA and BJ. The TB-mBJ results are in very good agreement with the experimental ones, with exception of *t*-ZrO_2 and Na_2ZrSiO_5. In these cases, the discrepancies with the experiments can be associated to the complexity of the samples and the presence of defects, impurities, and spurious phases.

From our results we conclude that the GIPAW methodology can predict the EFG at the Zr sites of these Zr-compounds with the same precision than FP-LAPW for identical geometries. Moreover, the predicted $Q(^{91}Zr)$ using GIPAW results is in very good agreement with the values obtained using the well-established FP-LAPW method, showing that GIPAW could be a valuable method for the calculation of the EFG in crystals. This is an important conclusion because the GIPAW method allows DFT calculations with a better computational efficiency. The validation of this method for the calculation of hyperfine parameters

opens the way to using it as an alternative to all-electron methods for many isotopes and, particularly, complex systems.

Declaration of competing interest

The authors declare that they have no known competing financial interests or personal relationships that could have appeared to influence the work reported in this paper.

Data availability

Data will be made available on request.

Acknowledgements

This work was partially supported by CONICET, Argentina (grant no. PIP 0039-2017) and UNLP (grants no. 11/X845 and X806/18).

References

[1] G. Schatz, A. Weidinger, Nuclear Condensed Matter Physics: Nuclear Methods and Applications, Wiley, New York, 1995.
[2] C.P. Slichter, Principles of Magnetic Resonance, Springer Berlin, Heidelberg, 1990, https://doi.org/10.1007/978-3-662-09441-9.
[3] P. Gütlich, E. Bill, A.X. Trautwein, Mössbauer Spectroscopy and Transition ϵ Metal Chemistry, Springer-Verlag, Berlin, Heidelberg, 2011.
[4] Y. Yoshida, G. Langouche, Mössbauer Spectroscopy - Tutorial Book, Springer, New York, 2013.
[5] L. Errico, M. Rentería, H.M. Petrilli, Cd in SnO: probing structural effects on the electronic structure of doped oxide semiconductors through the electric field gradient at the Cd nucleus, Phys. Rev. B 75 (2007), 155209.
[6] L. Errico, K. Lejaeghere, J. Runco, S.N. Mishra, M. Rentería, S. Cottenier, Precision of electric-field gradient predictions by density functional theory and implications for the nuclear quadrupole moment and its error bar of the ^{111}Cd 245 keV 5/2^{+} level, J. Phys. Chem. C 120 (2016), 23111.
[7] N.J. Stone, Table of nuclear magnetic dipole and electric quadrupole moments, Atomic Data Nucl. Data Tables 90 (2005) 75.
[8] N.J. Stone, Table of Nuclear Magnetic Dipole and Electric Quadrupole Moments, International Nuclear Data Committee, 2014 last accessed September 2021, https://www-nds.iaea.org/publications/indc/indc-nds-0658.pdf.
[9] N.J. Stone, Table of Nuclear Electric Quadrupole Moments, International Nuclear Data Committee, 2014 last accessed September 2021, https://www-nds.iaea.org/publications/indc/indc-nds-0650.pdf.
[10] N.J. Stone, Table of Nuclear Electric Quadrupole Moments, International Nuclear Data Committee, 2021. https://www-nds.iaea.org/nuclearmoments/.
[11] P. Pyykko, Year-2008 nuclear quadrupole moments, Mol. Phys. 106 (2008) 1965.
[12] H. Haas, S.P.A. Sauer, L. Hemmingsen, V. Kellö, P.W. Zhao, Quadrupole moments of Cd and Zn nuclei: when solid-state, molecular, atomic, and nuclear theory meet, EPL 117 (2017), 62001.
[13] H. Haas, J. Röder, J.G. Correia, J. Schell, A.S. Fenta, R. Vianden, E.M.H. Larsen, P. A. Aggelund, R. Fromsejer, L.B.S. Hemmingsen, Free molecule studies by perturbed γ-γ angular correlation: a new path to accurate nuclear quadrupole moments, Phys. Rev. Lett. 126 (2021), 103001.
[14] B.E.G. Lucier, Y. Huang, A review of ^{91}Zr solid-state nuclear magnetic resonance spectroscopy, Annu. Rep. NMR Spectrosc. 84 (2015) 233.
[15] O.B. Lapina, D.F. Khabibulin, V.V. Terskikh, Multinuclear NMR study of silica fiberglass modified with zirconia, Solid State Nucl. Magn. Reson. 39 (2011) 47.
[16] C. Degueldre, G. Kuri, M. Martin, A. Froideval, S. Cammelli, A. Orlov, J. Bertsch, M. A. Pouchon, Nuclear material investigations by advanced analytical techniques, Nucl. Instrum. Methods Phys. Res. B 268 (2010) 3364.
[17] B. Cox, Some thoughts on the mechanisms of in-reactor corrosion of zirconium alloys, J. Nucl. Mater. 336 (2005) 331.
[18] A. Meldrum, L.A. Boatner, R.C. Ewing, Nanocrystalline zirconia can Be amorphized by ion irradiation, Phys. Rev. Lett. 88 (2001), 025503.
[19] E.H. Kisi, C.J. Howard, Crystal structure of zirconia phases and their inter-relation, Key Engineering Ceramics 153 (1998) 1.
[20] J. Chevalier, What future for zirconia as a biomaterial? Biomaterials 27 (2006) 535.
[21] X.Q. Cao, R. Vassen, D. Stoever, Ceramic materials for thermal barrier coatings, J. Eur. Ceram. Soc. 24 (2004) 1.
[22] No easy solutions for aerospace, Nat. Mater. 15 (2016) 803.
[23] M.S. Islam, R.A. Davies, J.D. Gale, Proton migration and defect interactions in the $CaZrO_3$ orthorhombic perovskite: a quantum mechanical study, Chem. Mater. 13 (2001) 2049.
[24] M. Pollet, S. Marinel, Copper electrodes multilayer ceramic capacitors Part I the dielectric composition, J. Mater. Sci. 39 (2004) 1943.
[25] P. Stoch, J. Szczerba, J. Lis, D. Madej, Z. Pędzich, Crystal structure and ab- initio calculations of $CaZrO_3$, J. Eur. Ceram. Soc. 32 (2012) 665.
[26] I. Zeba, M. Ramzan, R. Ahmad, M. Shakil, M. Rizwan, M. Rafique, M. Sarfraz, M. Ajmal, S.S.A. Gillani, First-principles computation of magnesium doped $CaZrO_3$ perovskite: a study of phase transformation, bandgap engineering and optical response for optoelectronic application, Solid State Commun. 313 (2020), 113907.
[27] S.S.A. Gillani, R. Ahmad, M. Rizwan, M. Rafique, G. Ullah, C.B. Cao, H.B. Jin, Effect of magnesium doping on band gap and optical properties of $SrZrO_3$ perovskite: a first-principles study, Optik 191 (2019) 132.
[28] W. Dong, Xiaoping Chen, Yu Fan, Ye Wu, $Na_2CO_3/MgO/Al_2O_3$ solid sorbents for low-temperature CO_2 capture, Energy Fuels 29 (2015) 968.
[29] S. Kumar, S.K. Saxena, A comparative study of CO_2 sorption properties for different oxides, Mater, Renew. Sustain. Energy 3 (2014) 30.
[30] S. Umesh, V. Kumar Jayaraman, V. Dhanasekaran, P. Annigere, Enhanced sodium ion conduction in Al-substituted Na_2ZrO_3, Mater. Lett. 304 (2021), 130713.
[31] H.E. Mahnke, Introduction to PAC/PAD, Hyperfine Interact. 49 (1989) 77.
[32] E. Sjöstedt, L. Nordström, D.J. Singh, An alternative way of linearizing the augmented plane-wave method, Solid State Commun. 114 (2000) 15.
[33] G.K.H. Madsen, P. Blaha, K. Schwarz, E. Sjöstedt, L. Nordström, Efficient linearization of the augmented plane-wave method, Phys. Rev. B 64 (2001), 195134.
[34] C.J. Pickard, F. Mauri, All-electron magnetic response with pseudopotentials: NMR chemical shifts, Phys. Rev. B 63 (2001), 245101.
[35] M. Profeta, F. Mauri, C.J. Pickard, Accurate first principles prediction of ^{17}O NMR parameters in SiO_2: assignment of the zeolite ferrierite spectrum, J. Am. Chem. Soc. 125 (2003) 541.
[36] P. Giannozzi, O. Andreussi, T. Brumme, O. Bunau, M. Buongiorno Nardelli, M. Calandra, R. Car, C. Cavazzoni, D. Ceresoli, M. Cococcioni, N. Colonna, I. Carnimeo, A. dal Corso, S. de Gironcoli, P. Delugas, R.A. DiStasio Jr., A. Ferretti, A. Floris, G. Fratesi, G. Fugallo, R. Gebauer, U. Gerstmann, F. Giustino, T. Gorni, T. J. Jia, M. Kawamura, H.-Y. Ko, A. Kokalj, E. Kucukbenli, M. Lazzeri, M. Marsili, N. Marzari, F. Mauri, N.L. Nguyen, H.-V. Nguyen, A. Otero-de-la-Roza, L. Paulatto, S. Poncé, D. Rocca, R. Sabatini, B. Santra, M. Schlipf, A.P. Seitsonen, A. Smogunov, I. Timrov, T. Thonhauser, P. Umari, N. Vast, X. Wu, S. Baroni, Advanced capabilities for materials modelling with Quantum Espresso, J. Phys. Condens. Matter 29 (2017), 465901.
[37] P. Blaha, K. Schwarz, G. Madsen, D. Kvasnicka, J. Luitz, R. Laskowski, F. Tran, L. Marks, WIEN2k, in: K. Schwarz (Ed.), An Augmented Plane Wave Plus Local Orbitals Program for Calculating Crystal Properties, Techn, Universitat Wien, Austria, 2018.
[38] J.P. Perdew, Y. Wang, Accurate and simple analytic representation of the electron-gas correlation energy, Phys. Rev. B 45 (1992), 13244.
[39] J.P. Perdew, K. Burke, M. Ernzerhof, Generalized gradient approximation made simple, Phys. Rev. Lett. 77 (1996) 3865.
[40] Z. Wu, R.E. Cohen, More accurate generalized gradient approximation for solids, Phys. Rev. B 73 (2006), 235116.
[41] A.D. Becke, E.R. Johnson, A simple effective potential for exchange, J. Chem. Phys. 124 (2006), 221101.
[42] F. Tran, P. Blaha, Accurate band gaps of semiconductors and insulators with a semilocal exchange-correlation potential, Phys. Rev. Lett. 102 (2009), 226401.
[43] D. Koller, F. Tran, P. Blaha, Improving the modified Becke-Johnson exchange potential, Phys. Rev. B 85 (2012), 155109.
[44] P.E. Blöchl, Projector augmented-wave method, Phys. Rev. B 50 (1994), 17953.
[45] K. Lejaeghere, G. Bihlmayer, T. Björkman, P. Blaha, S. Blügel, V. Blum, D. Caliste, I. E. Castelli, S.J. Clark, A. Dal Corso, S. de Gironcoli, T. Deutsch, J.K. Dewhurst, I. Di Marco, C. Draxl, M. Dułak, O. Eriksson, J.A. Flores-Livas, K.F. Garrity, L. Genovese, P. Giannozzi, M. Giantomassi, S. Goedecker, X. Gonze, O. Grånäs, E.K.U. Gross, A. Gulans, F. Gygi, D.R. Hamann, P.J. Hasnip, N.A.W. Holzwarth, D. Iuşan, D. B. Jochym, F. Jollet, D. Jones, G. Kresse, K. Koepernik, E. Küçükbenli, Y. O. Kvashnin, I.L.M. Locht, S. Lubeck, M. Marsman, N. Marzari, U. Nitzsche, L. Nordström, T. Ozaki, L. Paulatto, C.J. Pickard, W. Poelmans, M.I.J. Probert, K. Refson, M. Richter, G.M. Rignanese, S. Saha, M. Scheffler, M. Schlipf, K. Schwarz, S. Sharma, F. Tavazza, P. Thunström, A. Tkatchenko, M. Torrent, D. Vanderbilt, M.J. van Setten, V. Van Speybroeck, J.M. Wills, J.R. Yates, G.-X. Zhang, S. Cottenier, Reproducibility in density functional theory calculations of solids, Science 351 (2016) aad3000.
[46] C. Bonhomme, C. Gervais, F. Babonneau, C. Coelho, F. Pourpoint, T. Azaïs, S. E. Ashbrook, J.M. Griffin, J.R. Yates, F. Mauri, C.J. Pickard, First-principles calculation of NMR parameters using the Gauge Including Projector Augmented Wave method: a chemist's point of view, Chem. Rev. 112 (2012) 5733.
[47] D. Richard, A.V. Gil Rebaza, The GIPAW approach for the study of local structures and the electric field gradients at Cd and Ta impurity sites. Application to doped yttria ceramics, Comput. Mater. Sci. 171 (2020), 109224.
[48] G. Prandini, A. Marrazzo, I.E. Castelli, N. Mounet, N. Marzari, Precision and efficiency in solid-state pseudopotential calculations, NPJ Comput. Mater. 4 (2018) 72.
[49] A. Dal Corso, Pseudopotentials periodic table: from H to Pu, Comput. Mater. Sci. 95 (2014) 337.
[50] J. Goldak, L.T. Lloyd, C.S. Barrett, Lattice parameters, thermal expansions, and grüneisen coefficients of zirconium, 4.2 to 1130°K, Phys. Rev. 144 (1966) 478.
[51] D.S. Easton, J.O. Betterton, The eutectoid region of the Zr—Ga system, Metall. Mater. Trans. B 1 (1970) 3295.
[52] P. Blaha, K. Schwarz, P.H. Dederichs, First principles calculations of the electric-field gradient in HCP metals, Phys. Rev. B 37 (1988) 2792.
[53] T. Hioki, M. Kontani, Y. Masuda, Nuclear magnetic resonance in zirconium metal, J. Phys. Soc. Jpn. 39 (1975) 958.
[54] P. Raghavan, M. Senba, A. Lopez-Garcia, L. Zamdick, R.S. Raghavan, Bull. Am. Phys. Soc. 26 (1981) 538.
[55] R. Vianden, Systematics of electric field gradients in metals, Hyperfine Interact. 15/16 (1983) 189.

[56] S. Büttgenbach, R. Dicke, H. Gebauer, R. Kuhnen, F. Träber, Hyperfine structure in 4d- and 5d-shell atoms, Springer Tr. Mod. Phys. 96 (1982) 78–86. Springer, Berlin.
[57] L. Young, C.A. Kurtz, D.R. Beck, D. Datta, Hyperfine-structure studies of ZrII: experimental and relativistic configuration-interactions results, Phys. Rev. 48 (1993) 173.
[58] S. Bouazza, J. Dembczynski, E. Stachowska, G. Szawiola, J. Ruczkowski, Reanalysis and semi-empirical predictions of the hyperfine structure of in the model space, Eur. Phys. J. A D4 (1998) 39.
[59] V. Kellö, P. Pyykkö, A.J. Sadlej, P. Schwerdtfeger, J. Thyssen, The nuclear quadrupole moment of ^{91}Zr from molecular data for ZrO and ZrS, Chem. Phys. Lett. 318 (2000) 222.
[60] P. Raghavan, M. Senba, Z.Z. Ding, A. Lopez-Garcia, B.A. Brown, R.S. Raghavan, E2 effective charges of $g_{9/2}$ nucleons derived from quadrupole moments of high-spin isomers in ^{89,90,91}Zr and ^{90,92,94}Mo, Phys. Rev. Lett. 54 (1985) 2592.
[61] J. Bendahan, C. Broude, E. Dafni, G. Goldring, M. Hass, E. Naim, M.H. Rafailovich, Signs of the quadrupole moments of the 8^+ isomers in $^{88,\ 90}$Zr, Phys. Rev. C 33 (1986) 1517.
[62] J. Christiansen, P. Heubes, R. Keitel, W. Klinger, W. Loeffler, W. Sandner, W. Witthuhn, Temperature dependence of the electric field gradient in noncubic metals, Z. Phys. B Condens. Matter 24 (1976) 177–187.
[63] D. Steele, B.E.F. Fender, The structure of cubic ZrO_2:$YO_{1.5}$ solid solutions by neutron scattering, J. Phys. C Solid State Phys. 7 (1974) 1.
[64] C.J. Howard, R.J. Hill, B.E. Reichert, Structures of ZrO_2 polymorphs at room temperature by high-resolution neutron powder diffraction, Acta Crystallogr. B 44 (1988) 116.
[65] B.A. Kolesov, C.A. Geiger, T. Armbruster, The dynamic properties of zircon studied by single-crystal X-ray diffraction and Raman spectroscopy, Eur. J. Mineral 13 (2001) 939.
[66] A.I. Lebedev, I.A. Sluchinskaya, Structural instability in BaZrO3 crystals: calculations and experiment, Phys. Solid State 55 (2013) 1941.
[67] A. Ahtee, M. Ahtee, A.M. Glazer, A.W. Hewat, The structure of orthorhombic $SrZrO_3$ by neutron powder diffraction, Acta Crystallogr. B32 (1976) 3243.
[68] Y. Duan, J. Lekse, X. Wang, B. Li, B. Alcántar-Vázquez, H. Pfeiffer, J.W. Halley, Electronic structure, phonon dynamical properties, and CO_2 capture capability of $Na_{2-x}M_xZrO_3$ (M=Li, K): density-Functional calculations and experimental validations, Phys. Rev. Applied 3 (2015), 044013.
[69] G. Wilson, F.P. Glasser, Powder X-Ray data for synthetic anhydrous sodium zirconium silicates, Powder Diffr. 2 (1987) 176.
[70] Ch Thierfelder, P. Schwerdtfeger, T. Saue, ^{63}Cu and ^{197}Au nuclear quadrupole moments from four-component relativistic density-functional calculations using correct long-range exchange, Phys. Rev. 76 (2007), 034502.
[71] B.A. Kolesov, C.A. Geiger, T. Armbruster, The dynamic properties of zircon studied by single-crystal X-ray diffraction and Raman spectroscopy, Eur. J. Mineral 13 (2001) 939.

A.V. Gil Rebaza[a,*], A.M. Mudarra Navarro[a], M.A. Taylor[a,b], L. A. Errico[a,c], S. Cottenier[d,e]

[a] *Departamento de Física, Facultad de Ciencias Exactas, UNLP, Instituto de Física La Plata IFLP, CONICET, CCT, 1900, La Plata, Argentina*

[b] *Departamento Ciencias Básicas. Facultad de Ingeniería, UNLP, 1900, La Plata, Argentina*

[c] *Universidad Nacional Del Noroeste de La Pcia. de Buenos Aires (UNNOBA), Pergamino CP 2700, Buenos Aires, Argentina*

[d] *Department of Electromechanical, Systems and Metal Engineering, Ghent University, Technologiepark 46, Zwijnaarde, BE-9052, Belgium*

[e] *Department of Electromechanical, Systems and Metal Engineering & Center for Molecular Modeling (CMM), Ghent University, Technologiepark-Zwijnaarde 46, BE-9052, Zwijnaarde, Belgium*

[*] Corresponding author. Departamento de Física - Facultad de Ciencias Exactas, Universidad Nacional de La Plata and Instituto de Física La Plata (IFLP, CONICET), CC 67, 1900, La Plata, Argentina.
E-mail address: arlesv@fisica.unlp.edu.ar (A.V. Gil Rebaza).